Monthly Notices
of the
ROYAL ASTRONOMICAL SOCIETY

Mon. Not. R. Astron. Soc. **425,** 2049–2057 (2012) doi:10.1111/j.1365-2966.2012.21553.x

A kinematic classification of the cosmic web

Yehuda Hoffman,[1⋆] Ofer Metuki,[1] Gustavo Yepes,[2] Stefan Gottlöber,[3] Jaime E. Forero-Romero,[3] Noam I. Libeskind[3] and Alexander Knebe[2]

[1]*Racah Institute of Physics, Hebrew University, Jerusalem 91904, Israel*
[2]*Grupo de Astrofísica, Universidad Autónoma de Madrid, Madrid E-28049, Spain*
[3]*Leibniz-Institut für Astrophysik Potsdam (AIP), An der Sternwarte 16, D-14482 Potsdam, Germany*

Accepted 2012 June 19. Received 2012 May 10; in original form 2011 August 25

ABSTRACT

A new approach for the classification of the cosmic web is presented. In extension of the previous work of Hahn et al. and Forero-Romero et al., the new algorithm is based on the analysis of the velocity shear tensor rather than the gravitational tidal tensor. The procedure consists of the construction of the shear tensor at each (grid) point in space and the evaluation of its three eigenvectors. A given point is classified to be either a void, sheet, filament or a knot according to the number of eigenvalues above a certain threshold, 0, 1, 2 or 3, respectively. The threshold is treated as a free parameter that defines the web. The algorithm has been applied to a dark matter only simulation of a box of side length $64\,h^{-1}$ Mpc and $N = 1024^3$ particles within the framework of the 5-year *Wilkinson and Microwave Anisotropy Probe*/Λ cold dark matter (ΛCDM) model. The resulting velocity-based cosmic web resolves structures down to $\lesssim 0.1\,h^{-1}$ Mpc scales, as opposed to the $\approx 1\,h^{-1}$ Mpc scale of the tidal-based web. The underdense regions are made of extended voids bisected by planar sheets, whose density is also below the mean. The overdense regions are vastly dominated by the linear filaments and knots. The resolution achieved by the velocity-based cosmic web provides a platform for studying the formation of haloes and galaxies within the framework of the cosmic web.

Key words: cosmology: theory – dark matter – large scale of Universe.

1 INTRODUCTION

The visual appearance of the large-scale structure (LSS) of the Universe is of a web, the so-called cosmic web (Bond, Kofman & Pogosyan 1996). The large-scale distribution of galaxies in the observed Universe as well as the distribution of the dark matter (DM) as inferred from its gravitational lensing and reconstructions from large galaxy surveys give the appearance of mass and light distributed in a web-like structure dominated by linear filaments and concentrated compact knots, thereby leaving behind vast extended regions of no or a few galaxies and of low density (Kitaura et al. 2009; Jasche et al. 2010; Muñoz-Cuartas, Mueller & Forero-Romero 2011; Wang et al. 2012). Direct mapping of the mass distribution by weak lensing reveals a time-evolving loose network of filaments, which connects rich clusters of galaxies (Massey et al. 2007). The extreme low resolution of the weak lensing maps cannot reveal the full intricacy of the cosmic web, and in particular the difference between filaments and sheets, yet they reveal a web structure that serves as a gravitational scaffold into which gas can accumulate, and stars can be built. This poses an intriguing challenge of the mathematical classification and quantification of the cosmic web. The motivation for such an endeavour is twofold. On the one hand, the cosmic web is there and so we want to describe it mathematically. On the other hand, the web classification might provide some extra parameters that quantify the environment within which DM haloes and galaxies form. The properties of galaxies are observed to depend on their environment (Dressler 1980; Avila-Reese et al. 2005; Blanton et al. 2005; Gao, Springel & White 2005; Maulbetsch et al. 2007; Forero-Romero et al. 2011). Furthermore, the dynamics of subhaloes and satellite galaxies suggests a possible dependence on the environment within which their parent haloes reside (Knebe et al. 2004; Libeskind et al. 2005, 2011). A web classification might extend our theoretical tools for understanding such a dependence.

Translating the visual impression of a cosmic web into a mathematical formulation is not trivial. The thorough review of Colberg et al. (2008) of void finders provides some perspective to the general issue of web classifiers. This has been pursued along two different lines: the geometric and the dynamic approaches. The geometric approach focuses on the point process exhibited by, say, the distribution of galaxies or DM haloes in simulations and describes it mathematically. This has been often applied independently of any dynamical context (Lemson & Kauffmann 1999; Novikov, Colombi & Doré 2006; Aragón-Calvo et al. 2007; Sousbie et al. 2008). The

⋆E-mail: hoffman@huji.ac.il

dynamic approach has its roots in the seminal work of Zeldovich (1970), which led to the 'Russian school of structure formation' (e.g. Arnold, Shandarin & Zeldovich 1982; Klypin & Shandarin 1983). The Zeldovich approximation has been the first analytical tool that enables the tracking of the formation of aspherical objects, thereby accounting for the formation of voids, sheets, filament and knots. A recent application of that approach to the cosmic web is presented in Lee & Lee (2008).

The geometric approach uses objects (galaxies or DM haloes) which are per definition at a position of locally high density. Hahn et al. (2007) proposed a very attractive dynamic classification of the cosmic web. They presented an algorithm by which each point in space can be classified as being either a void, sheet, filament or a knot point. Namely, an attribute is assigned at each point in space much in the same way as it is characterized by its density and velocity. This attribute depends, in turn, on the dynamics of the LSS, namely on the density and/or the velocity fields.

The Hahn et al. (2007) dynamic web classification is based on counting the number of positive eigenvalues of the tidal tensor, i.e. the Hessian of the gravitational potential. The number ranges over 0, 1, 2 and 3, corresponding to a void, sheet, filament and a knot attribute, respectively. This web classifier is of a dynamic nature, and it is closely related to the equations of motion that dictate the dynamics of the growth of structure. One can consider the web classifier to be a dynamical field that characterizes the LSS of the Universe, a field that accepts only four possible numbers. This approach is driven by the Zeldovich approximation, and its web classification agrees remarkably well with the visual impression one has in viewing the LSS on linear and quasi-linear scales, i.e. scales larger than a few megaparsecs. However, in going down to smaller scales, the Hahn et al. approach fails to recover the fine web exhibited by high-resolution numerical simulations. A partial remedy to this shortcoming was provided by Forero-Romero et al. (2009, hereafter FR09), who relaxed the assumption of the null threshold which is used to classify the web. FR09 argue that the value of the properly normalized threshold should be around unity. Indeed, the cosmic web defined by a non-zero threshold provides a much better description on the non-linear cosmic web, down to the megaparsec scale.

Inspection of high-resolution N-body simulations reveals a web-like structure on very small scales as well. In simulations aimed at resolving galactic scale haloes, the web is observed down to the virial radius of such haloes (Libeskind et al. 2011). Studying such simulations we have tried to extend the approach of FR09 down to sub-megaparsec scales, but have failed. Namely, the method has not been able to resolve the fine web of these scales.

In the linear regime of the gravitational instability, the velocity and gravitational fields are essentially identical, up to some scaling that depends on the cosmological parameters. Hence, the web classification of Hahn et al. (2007) and FR09 can be reformulated in terms of the (velocity) shear tensor. It follows that in the linear regime, the tidal tensor based cosmic web and the velocity tensor based web are identical (hereafter these are defined as T-web and V-web, respectively). Going to the fully non-linear regime, we expect the T-web and V-web to depart. Here, we study the cosmic web as revealed by studying the analysis of the fully non-linear velocity field. The algorithm proposed here is tested against a high-resolution DM-only N-body simulation.

A general remark is due here before proceeding to the main body of the paper. By itself, the cosmic web is an ill-defined entity. The transition from knots to filaments, sheets and voids seems to be smooth and gradual; yet visual impression strongly suggests that the LSS is correctly characterized by a cosmic web. This resonates somewhat with the issue of DM haloes. Again, visual impression strongly suggests that the dynamics of gravitational instability leads to the formation of bound compact entities called DM haloes, yet these objects have no strict boundaries and therefore their definition would rely on somewhat arbitrarily chosen free parameter(s). However, even if the gravitational collapse in an expanding Universe is still not fully understood, a lot of insight and understanding are provided by the spherical top-hat collapse model (Gunn & Gott 1972; Binney & Tremaine 1987). It follows that the majority of halo finders are based on the model and the free parameter that defines a given halo finder, e.g. the mean density of a halo or the linking length that defines friends-of-friends haloes is derived from the top-hat model. No such model exists that can provide a quantitative estimation of the value of one or more parameters that define the web. Hence, web classifier algorithms are bound to depend on some free parameters that cannot be determined from first principles. The web that emerges from the geometric web classifiers depends strongly on the type or properties of objects used to trace the web, such as the mass of DM haloes in simulations or the luminosity and spectral type of observed galaxies. The web that emerges from the dynamic web classification depends on the chosen smoothing, i.e. resolution, and the value of the adopted threshold. No attempt is made here to optimize the values of these two parameters as the optimization depends on the specific problem one wishes to address with the V-web. Different problems end up with different 'best' parameters. We have chosen to use parameters that are best suited for the simulation studied here and the visual impression it leads to.

This paper consists of a description of the algorithm that classifies the cosmic web (Section 2), a brief summary of the N-body simulation used here (Section 3) and a presentation of the results (Section 4). The paper concludes with a discussion of the V-web classification and its merits with respect to the analysis of structure and galaxy formation.

2 WEB CLASSIFICATION: ALGORITHM

Consider a DM-only N-body simulation. A description of the simulation can be provided by the density and velocity fields evaluated on a finite grid, $\rho(\boldsymbol{r})$ and $\boldsymbol{v}(\boldsymbol{r})$. The T-web is defined by the eigenvalues of the Hessian of the gravitational potential which obeys the (rescaled) Poisson equation:

$$\nabla^2\phi = \Delta. \tag{1}$$

Here, ϕ is the gravitational potential rescaled by $4\pi G\bar{\rho}$, $\bar{\rho}$ is the mean cosmological density and the density (ρ) is given by $\Delta = \rho/\bar{\rho}$. The tidal tensor is defined as the Hessian of ϕ, namely

$$T_{\alpha\beta} = \frac{\partial^2\phi}{\partial r_\alpha \partial r_\beta}, \tag{2}$$

where α and β represent x, y and z. The three eigenvalues of the tidal tensor are denoted here by $\lambda_i^{\rm T}$, where $i = 1, 2$ and 3. (Throughout the paper it is assumed that the eigenvalues are arranged in decreasing order.) Note that

$$\Delta(\boldsymbol{r}) = \lambda_1^{\rm T}(\boldsymbol{r}) + \lambda_2^{\rm T}(\boldsymbol{r}) + \lambda_3^{\rm T}(\boldsymbol{r}). \tag{3}$$

The V-web is defined in terms of the shear tensor, which is rescaled here and is written as

$$\Sigma_{\alpha\beta} = -\frac{1}{2}\left(\frac{\partial v_\alpha}{\partial r_\beta} + \frac{\partial v_\beta}{\partial r_\alpha}\right) \Big/ H_0, \tag{4}$$

where H_0 is the Hubble constant. The eigenvalues of $\Sigma_{\alpha\beta}$ are denoted here as $\lambda_i^{\rm V}$ ($i = 1, 2$ and 3).

The T-web and V-web are classified here by the number of the eigenvalues above a threshold, $\lambda_{\rm th}^{\rm T}$ and $\lambda_{\rm th}^{\rm V}$. We have not attempted to determine the values of these thresholds but rather to treat them as free parameters which define the corresponding webs. Our guiding principle is to adopt values which best reproduce the visual impression of the cosmic web.

3 SIMULATION

The web classification is applied here to a simulation performed under the framework of the Constrained Local Universe Simulations (CLUES) project,[1] whose aim is to perform cosmological simulations that reproduce the local LSS in the Universe as accurately as current observation admits. The simulation is performed within the Λ cold dark matter (ΛCDM) cosmology, with cosmological parameters consistent with a 5-year *Wilkinson Microwave Anisotropy Probe* (*WMAP*5) cosmology: a density parameter $\Omega_{\rm m} = 0.28$, a cosmological constant $\Omega_\Lambda = 0.72$, a dimensionless Hubble parameter $h = 0.70$, a spectral index of primordial density perturbations $n = 0.96$ and a normalization $\sigma_8 = 0.817$. The constrained nature of the simulation is ignored here, and it is treated as a typical realization of the ΛCDM/*WMAP*5 cosmology.

This is a pure DM simulation performed by the GADGET2 code within a computational box with side length $L_{\rm box} = 64\,h^{-1}$ Mpc using 1024^3 particles, corresponding to a particle mass of $m_{\rm p} = 1.839 \times 10^7\,h^{-1}\,{\rm M}_\odot$. The density and velocity fields are evaluated on a 256^3 grid, using clouds in cells (CIC) interpolation. Two CIC constructions are used here, the full computational box (BOX64) and an inner box of side length $8\,h^{-1}$ Mpc (BOX8) placed at the centre of the computational box. The CIC interpolation of the velocity field is performed by number weighting over the particles in adjacent cells. Differentiation of the velocity field is performed in Fourier space, using FFT. The CIC procedure smoothes the field under consideration over two grid units, and therefore no aliasing is introduced by the FFT transform.

4 RESULTS

Fig. 1 presents the analysis of the LSS delineated by one of the principal planes of the simulation. The analysis is applied to the BOX64 CIC field with a grid resolution of $0.25\,h^{-1}$ Mpc. Both the density and velocity fields have been Gaussian smoothed with a kernel of $R_{\rm s} = 0.25\,h^{-1}$ Mpc so as to suppress numerical artefacts on the grid scale, in particular the unphysical preferred directions induced by the Cartesian grid. The top panels show the (scaled) density field, $\Delta(\boldsymbol{r})$, in log (left) and linear (right) scales. The log scale map clearly distinguishes between the underdense and overdense regions. The middle panels show the V-web (left) and T-web (right). The threshold values used here are $\lambda_{\rm th}^{\rm V} = 0.44$ and $\lambda_{\rm th}^{\rm T} = 0.7$. The threshold values of the two webs have been chosen so as to obtain the maximal spatial resolution and to provide the best visual match to the appearance of the density field.

The grey scaling of the web maps is the following: white (voids), light grey (sheets), dark grey (filaments) and black (knots). It should be noted that the maps shown here represent planar cuts, namely slices of one grid cell ($0.25\,h^{-1}$ Mpc) thickness, through a 3D structures; hence the sheets appear as roughly 1D filamentary objects, while the filaments appear as isolated spots, reminding the appearance of the knots. The bottom-right panel shows the negative of the divergence of the velocity fields, namely the sum of $\lambda_i^{\rm V}$ at each grid point.

Inspection of the different plots of Fig. 1 reveals a rich cosmic web. A few immediate conclusions follow.

(i) The V-web provides a much superior description of the web structure that is revealed by the mass distribution, compared with the T-web. This is best exemplified by the dense object at $(X, Y, Z) \approx (-2,\ 12,\ 0)\,h^{-1}$ Mpc. The V-web reveals the delicate structure around the object, while the T-web yields an unresolved blob over there. In fact, the T-web shown in the figure has been constructed with an optimal choice of the smoothing and threshold parameters, so as to achieve the maximum spatial resolution. In particular, a reduction in the Gaussian smoothing does not lead to an improvement in the resolution of the T-web.

(ii) The web permeates through the underdense regions, where large extended almost empty regions are bisected by sheets.

(iii) The sheets prevail mostly in the underdense regions, compared with the filaments and knots which dominate the overdense regions.

(iv) Some of the sheets located in the underdense regions exhibit a two-caustic structure enclosing a void region. Namely, an inner planar part has a diverging velocity field ($\nabla \cdot \boldsymbol{v} \geq 0$) that is sandwiched between two caustics with a converging velocity field ($\nabla \cdot \boldsymbol{v} < 0$). Such double sheets appear only in the underdense regions.

(v) The velocity divergence field follows very closely the density field, with almost a complete match of the underdense with the positive $-\nabla \cdot \boldsymbol{v}$ regions. Such a correspondence is the key for the success of the V-web in tracing the density field. Note that in the linear theory of gravitational instability, underdense points are always associated with a divergent flow. It follows that the emergence of underdense regions with converging flows is a pure non-linear dynamical effect. The present V-web algorithm classifies these objects as sheets.

Figs 2 and 3 present a zoom on the inner $(8\,h^{-1}\,{\rm Mpc})^3$ of the simulation, showing the density fields in linear and log scale and the V-web at a Gaussian smoothing of $R_{\rm s} = 0.125\,h^{-1}$ Mpc. The density and velocity fields have been CIC-ed on a 256^3 grid spanning the zoom region. The figures show parallel slices of $Z = -3$, -2, -1, 0, 1, 2 and $3\,h^{-1}$ Mpc so as to depict the 3D structure. The colour coding of the density (linear scale) field has been chosen so as to make the structure at the $\Delta(\boldsymbol{r}) \approx 1$ level more apparent. The log scale density maps provide a clear presentation of the overdense regions. The 3D structure that emerges from these parallel plots is of a filament that runs roughly parallel to the Z-axis across the slices presented here. The width of the filament depends somewhat on the value of the threshold used to define the web. The threshold also dictates whether the filament appears monolithic or if it breaks into smaller parallel filaments. That filament is embedded within a curvy wall, i.e. sheet, of $\Delta(\boldsymbol{r}) \approx 1$ that runs across the slices from $Z = -3$ to $3\,h^{-1}$ Mpc. The wall leaves its trace on the parallel planes as a (partial) horseshoe linear structure running from $(X,\ Z) \approx (-0.5,\ -4)\,h^{-1}$ Mpc through $\approx(0,\ 0)$ towards $\approx(4,\ 3)\,h^{-1}$ Mpc. That wall is clearly classified by the V-web as a sheet, and it is clearly visible in the (linear scale) density maps. The wall borders a coherent underdense region on the bottom-right quarter of all the parallel planes. Now this underdense region, which runs parallel to the Z-axis, is not monolithic. It is further split by density ridges, forming some more smaller scale sheets that cut through

[1] http://www.clues-project.org/

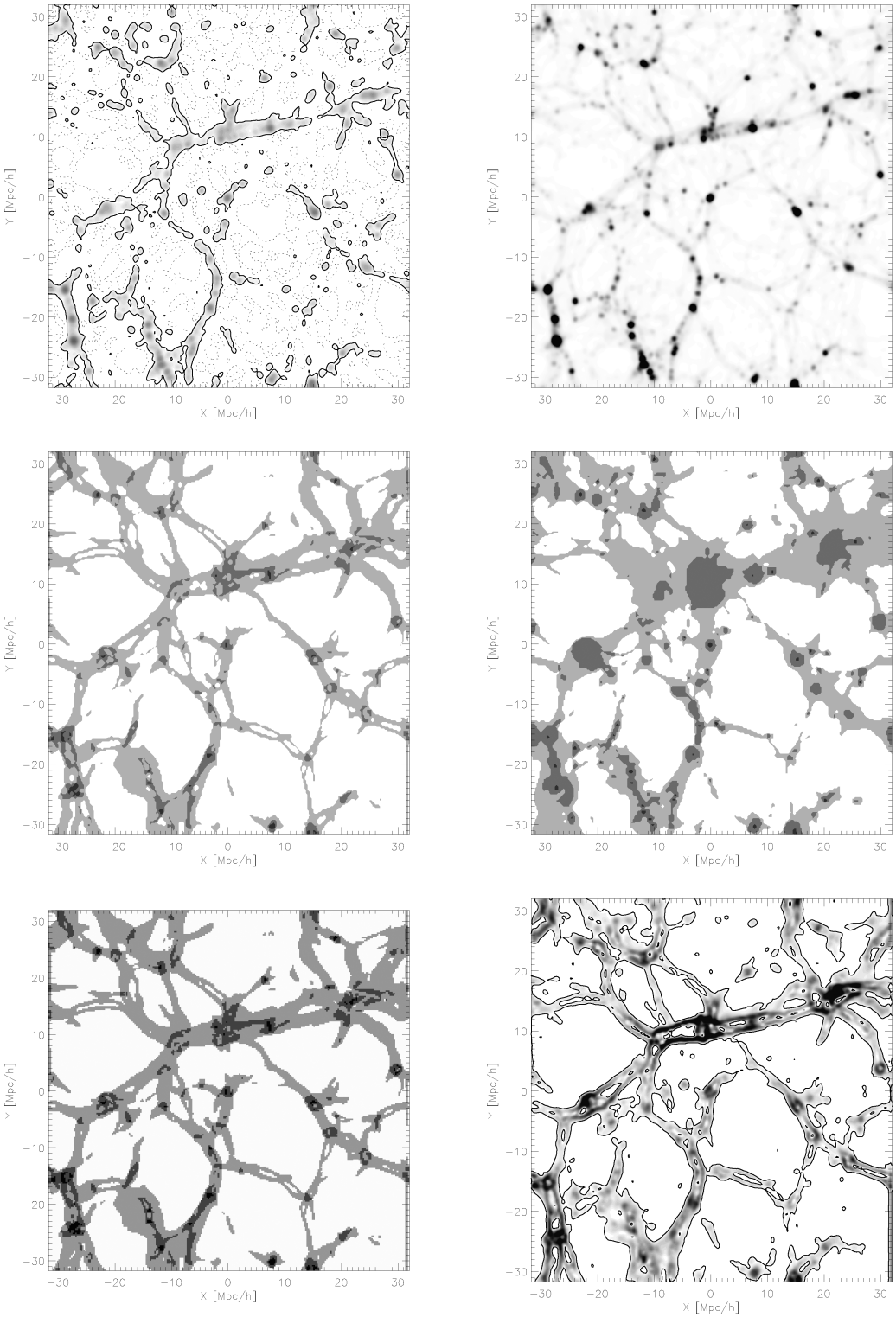

Figure 1. The normalized density field and the cosmic web, based on the CIC density field of the full computational box (BOX64) spanned on a 256^3 grid and Gaussian smoothed on the scale of $0.25\,h^{-1}$ Mpc. (a) The density field presented by $\log\Delta$ (grey-scale corresponds to overdense region, and dashed contours to underdense region. The solid contour represents the mean density (top-left panel). (b) The linear density field (represented by grey-scale colour map; top-right panel). (c) The velocity-based cosmic web generated with $\lambda_{\rm th}^{\rm V} = 0.44$ made of voids (white), sheets (light grey), filaments (dark grey) and knots (black). Note that the map presents a planar cut through the cosmic web; hence, sheets appear as long filaments and filaments as isolated compact regions (middle left panel). (d) The (gravitational) tidal cosmic web generated with $\lambda_{\rm th}^{\rm T} = 0.7$ (same colour coding for the cosmic web, middle right panel). (e) The multiscale-corrected V-web (see Section 5, bottom-left panel). (f) The divergent of the velocity field: the grey-scale shading corresponds to $-\nabla\cdot\boldsymbol{v} \geq 0$ (bottom-right panel).

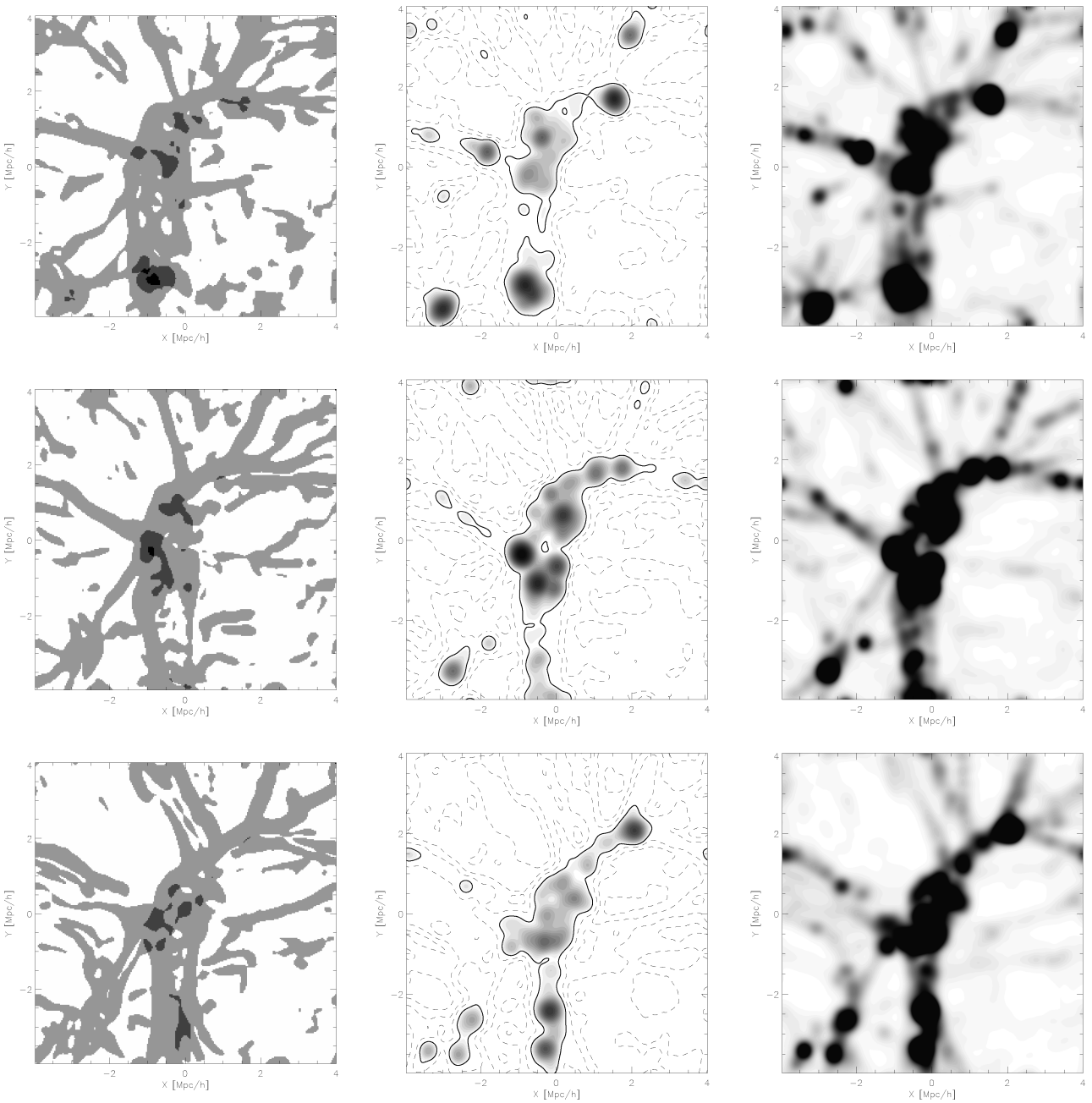

Figure 2. Zoom on the centre of the computational box showing the density fields in linear and log scale and the V-web at a Gaussian smoothing of $R_s = 0.125\,h^{-1}$ Mpc. Each row contains the V-web (left), log scale density (middle) and linear density field (right) maps. The top, middle and bottom rows correspond to the $Z = 3, 2, 1\,h^{-1}$ Mpc planes, respectively. (The colour coding and threshold values of Fig. 1 are followed here.)

the underdense big blob creating smaller voids. These ridges are underdense themselves, yet they are denser than the voids they surround. Some other coherent voids, sheets and filaments that run perpendicular to the $Z =$ constant planes are apparent as well.

The two middle panels of Fig. 1, which depict the V-web and T-web, clearly show that the improved spatial resolution of the V-web compared with the T-web. The comparison is further extended in Fig. 4. Again, lacking a quantitative measure of the quality of the construction of the cosmic web, we resort here to a visual comparison of the constructed cosmic web with the underlying density field. The plots show the *XZ* plane of the zoom box presented in the series of the *Z* cuts of Figs 2 and 3. The sheet that almost coincides with the *YZ* principle plane is clearly manifested in the orthogonal *XZ* cut. The plots also show the filament that runs very close to the *Z*-axis. The fine details, on sub-megaparsec scale, of the density field are much better reproduced by the V-web than by the T-web.

5 SOME STATISTICS AND A MULTISCALE APPROACH

A close inspection of the density and V-web maps (Figs 1–4) shows a very clear correlation of the V-web classification with the local density. There is clear correspondence between the web type with density, with voids, sheets, filaments and knots progressing from the most underdense to the densest environments, respectively. Yet,

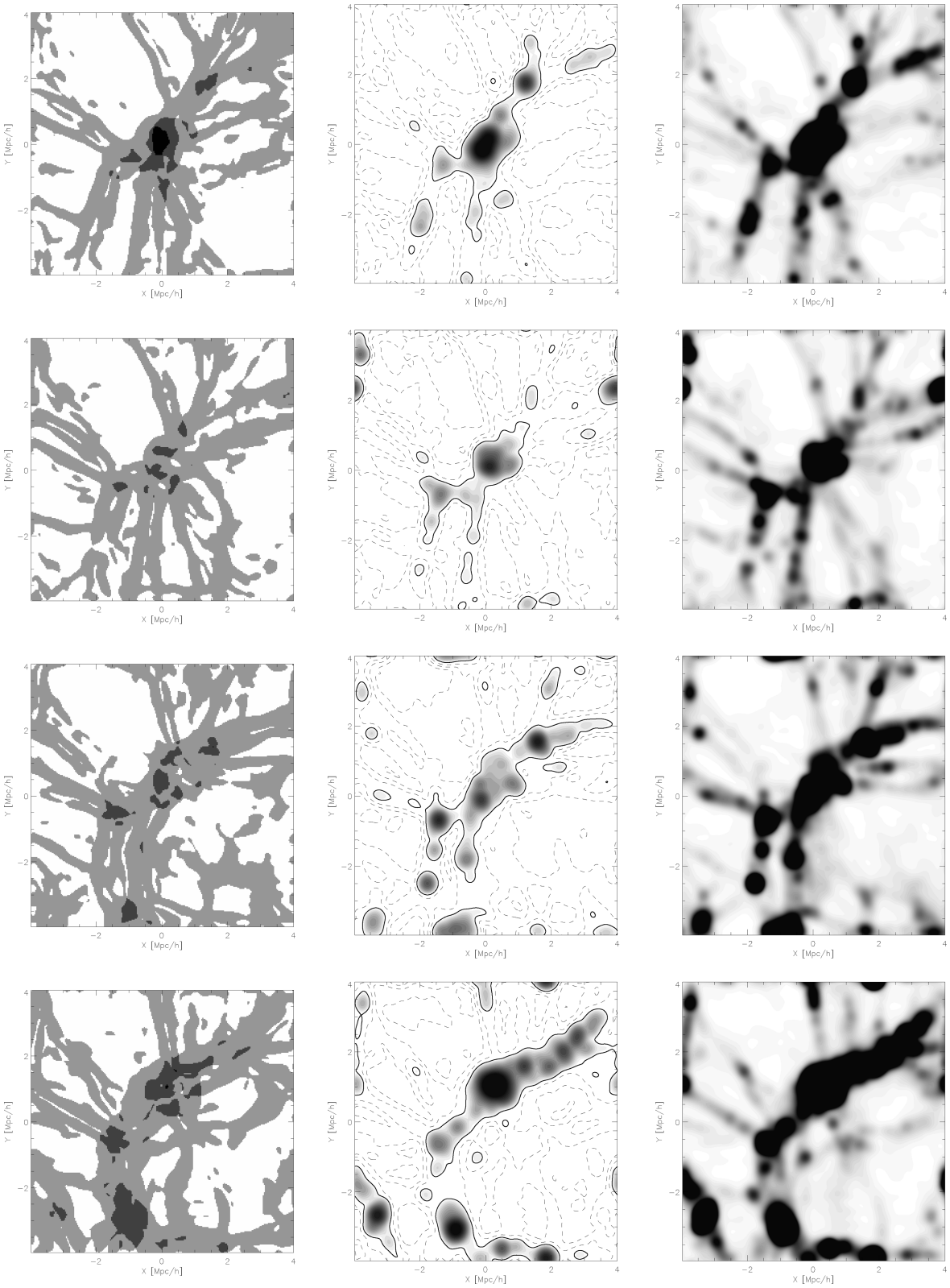

Figure 3. Same as Fig. 2, for $SGZ = 0$, -1, -2 and $-3\,h^{-1}$ Mpc.

there is no one-to-one correspondence between the web type and density, as is manifested by Fig. 5, whose left-hand panel shows the probability distribution of grid cells for the different web elements as a function of the fractional density, Δ. The plot shows that virtually at all density levels, cells of any web type can be found. In particular, some very dense cells with $\Delta \approx 10^3$ are tagged as voids. A close inspection reveals that all such points are located at the very inner regions of massive haloes, where the velocity field reflects the virial

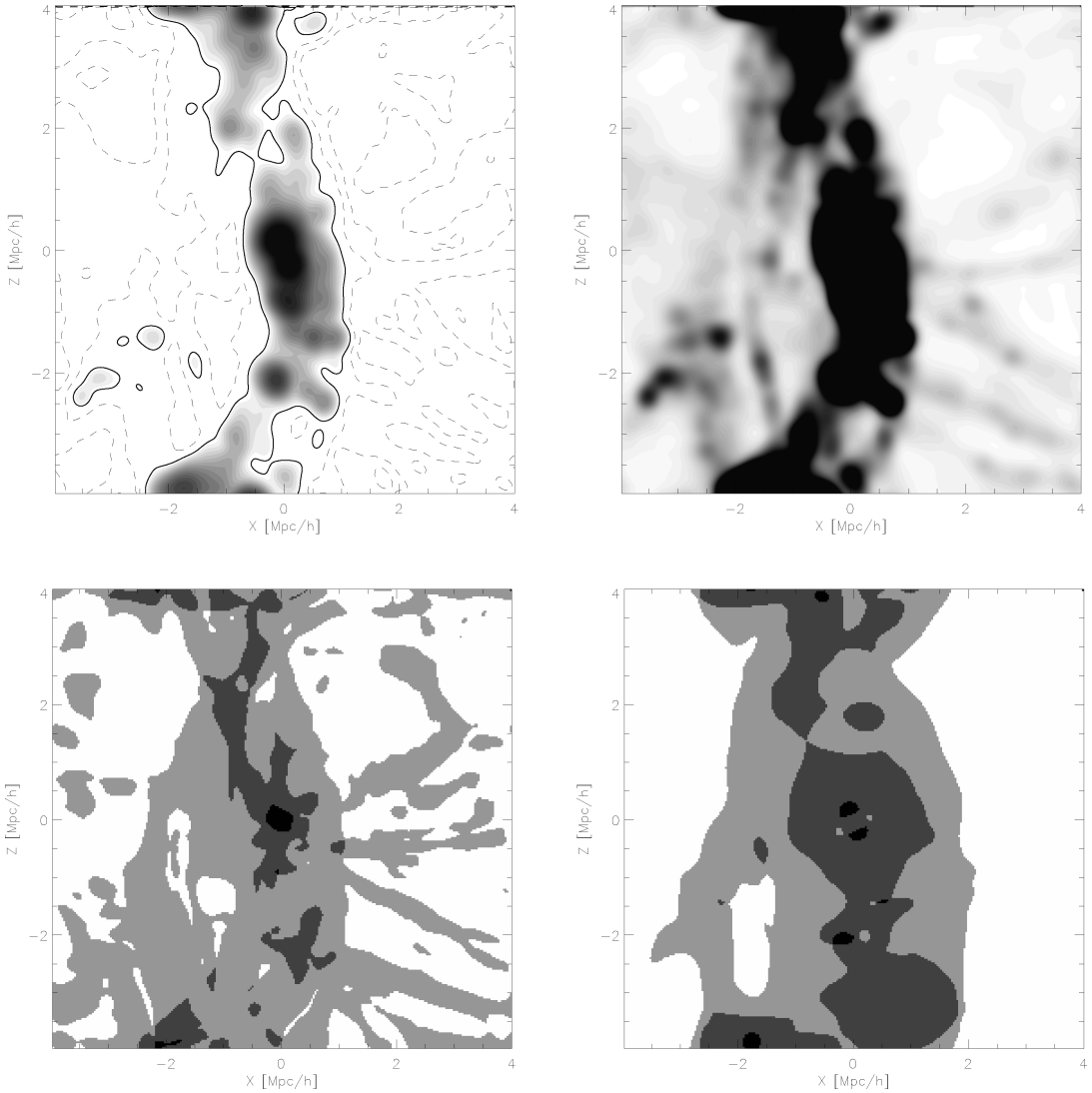

Figure 4. A comparison of the V-web and T-web of the *XZ*-plane of the zoom box (shown in Figs 2 and 3, using the same resolution and threshold values of Fig. 1). (a) The density field presented by log Δ (top-left panel). (b) The linear density field (top-right panel). (c) The velocity-based cosmic web (bottom-left panel). (d) The (gravitational) tidal cosmic web (bottom-right panel). The colour and contour coding of Fig. 1 is followed here.

motions within virialized haloes. This is a clear artefact of the over-resolution of the CIC grid which penetrates too deeply into massive haloes. Only a very few cells are affected by this over-resolution, and the global statistics is virtually unaffected. A similar effect is found also for some of the cells with density exceeding the virial mean density ($\Delta \approx 340$ for the cosmological parameters assumed here), which are classified as sheets and filaments, and are clearly located within the very inner regions of massive haloes. The over-resolution conjecture is easily verified by constructing a lower resolution V-web and confirming that the pathology disappears with the coarser grid.

The following multiscale procedure effectively removes the pathological misclassified cells. A low-resolution V-web is constructed, in addition to the finest desired web. All high-resolution cells that are defined as voids and have an overdensity exceeding unity, $\Delta \geq 1$, are given the web attributes of the coarse web. Similarly, all high-resolution cells identified as sheets and filaments whose overdensity exceeds the virial density assume the web classification of the coarse grid. Both the high- and low-resolution webs are evaluated on the same 256^3 grid, and the resolution is controlled by a Gaussian smoothing. The coarse grid is defined here by a Gaussian smoothing of $R_g = 1\,h^{-1}$ Mpc. The probability distribution of grid cells of the corrected web is shown by the right-hand panel of Fig. 5. The corrected V-web is presented by the bottom-left panel of Fig. 1. From here on the V-web is assumed to be corrected by the multiscale approach, unless it is otherwise explicitly stated.

Table 1 presents the volume and mass filling factors of the V-web. The numbers in parentheses correspond to the V-web constructed without the multiscale correction. The numbers presented here clearly depend on the threshold level and resolution. Given that the V-web calculated here closely matches the visual appearance implied by the mass distribution, the following remarks are of interest. Voids and sheets occupy 95 per cent of the simulated volume, and only less than 1 per cent is occupied by knots. The volume and mass filling factors of the sheets and filaments are in close agreement with the findings of FR09, for a threshold of unity. The sheets are more dominant by volume and mass in the V-web compared with the T-web.

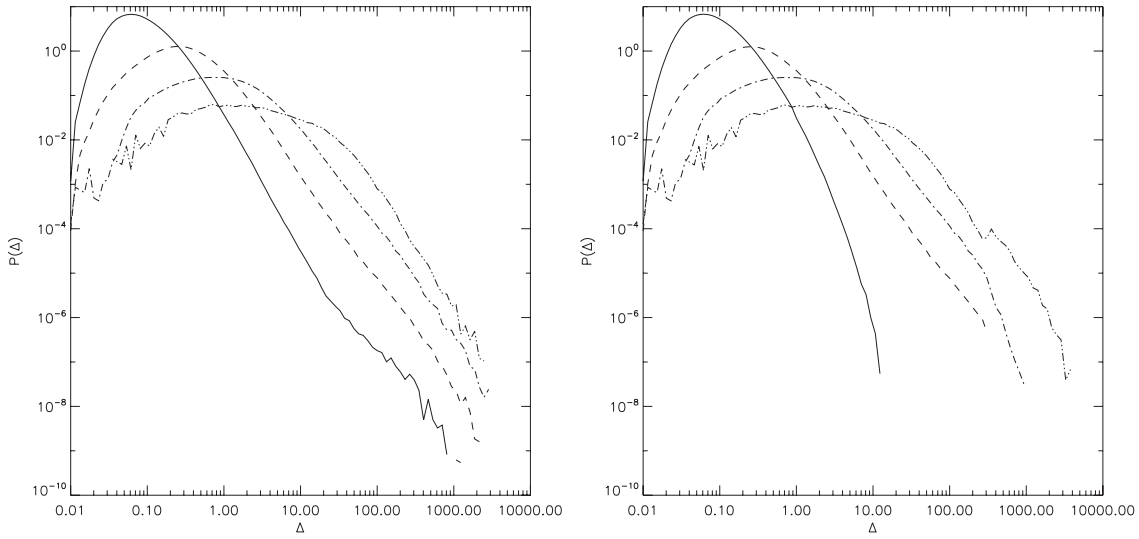

Figure 5. The probability distribution of grid cells as a function of the fractional density, $P(\Delta)$, is plotted for the various V-web elements, voids (full line), sheets (dashed), filaments (dot–dashed) and knots (double-dot–dashed). The left-hand panel shows the distribution for V-web calculated with a Gaussian smoothing of $R_s = 0.25\,h^{-1}$ Mpc. The right-hand panel shows the distribution after applying the multiscale correction.

Table 1. The volume and mass filling factors of the various web elements. The filling factors obtained without the multiscale correction are given in parentheses.

Web elements	Volume filling fraction	Mass filling fraction
Voids	0.68 (0.69)	0.13 (0.15)
Sheets	0.27 (0.26)	0.36 (0.37)
Filaments	0.046 (0.046)	0.34 (0.37)
Knots	0.0036 (0.0035)	0.17 (0.11)

6 DISCUSSION

A novel algorithm for classifying the cosmic web has been introduced here. The algorithm extends the dynamic classification of Hahn et al. (2007) and FR09 by studying the eigenvalues of the (velocity) shear tensor at any given point rather than those of the (gravitational) tidal tensor. The web classification depends on the number of eigenvalues above a given threshold. Each point is classified as either a void (0 eigenvectors above the threshold), sheet (1), filament (2) or a knot (3). The value of the threshold is taken as a free parameter, determined so as to provide the best visual match to the observed LSS. As was pointed out in Section 1, there is no model which can make quantitative predictions of the cosmic web at the current epoch non-linear universe. This renders the various cosmic web finders to depend on one or more free parameters that cannot be derived from first principles. The V-web, defined by the threshold and by the adopted resolution, can serve as a platform for studying, among other things, the properties of galaxies and haloes with respect to their environs. The choice of the parameters defining the web needs to be optimized according to the problem at hand. The focus of the present paper is on the presentation of the method, choosing the threshold and resolution parameters so as to recover the visual impression that emerges from the LSS of the simulation. Detailed study and analysis of the cosmic web and its relation to the properties of DM haloes and simulated galaxies are to be presented in a forthcoming series of papers. In particular, future studies will focus on studying within the CLUES framework the Local Group in the context of the local cosmic web. A first step in that direction is the study of the orientation of the angular momentum of parent and subhaloes with respect to the cosmic web (Libeskind et al. 2012).

Figs 1–3 clearly show that the kinematic cosmic web (V-web) resolves much smaller structure than the gravitational cosmic web (T-web). The two possible definitions of the web coincide on the large scales, where the linear regime prevails, but they depart at small scales, where the non-linear dynamics manifests itself. Why does the velocity field trace the underlying cosmic web better? The following argument might provide a plausible explanation. It is known that the skeleton of the cosmic web has already been delineated by the initial conditions (Zeldovich 1970; Bond et al. 1996). It is also well known that the density field, and hence also the gravity field, evolves away from the linear regime faster than the velocity field (Kitaura et al. 2011, and references therein). This suggests that the velocity field retains a better memory of the initial conditions than the gravitational field, and therefore is expected to trace the cosmic web better. The present calculations support that assertion, yet the problem deserves a more in-depth study.

The cosmic web permeates the LSS (Bond et al. 1996), covering all regimes from the very underdense to the densest regions. Although the cosmic web correlates with the matter density, it cannot be solely described by the local density. For example, vast underdense regions are bisected by planar structures (e.g. Aragon-Calvo & Szalay 2012) that are clearly manifested by the matter distribution and are tagged as sheets by the V-web finder. The underdense blobs, $\Delta < 1.0$, are surrounded by 2D sheets with $\Delta \approx 1.0$. Sheets contain quasi-linear partially collapsed 1D filaments, which in turn contain highly non-linear compact knots. Fig. 5 shows that the sheets are associated with the quasi-linear density field. The DM halo mass function has a strong dependence on the ambient density, and the mass function of haloes residing in low-density regions is heavily skewed towards low-mass haloes (Lemson & Kauffmann 1999; Hahn et al. 2007). Hence, sheets are expected to be populated by low-mass haloes and therefore to host predominantly faint galaxies. It follows that magnitude-limited redshift surveys of galaxies which trace the distribution of the more luminous galaxies are expected to be biased towards the luminous knots and filaments, leaving behind the dimmer sheets to be virtually undetected. As telescopes become more and more sensitive and begin to probe dimmer and dimmer

galaxies, the internal structure of underdense cosmic web types (i.e. voids and sheets) will come into focus.

ACKNOWLEDGMENTS

Fruitful discussions with Francisco-Shu Kitaura are gratefully acknowledged. This research has been partially supported by the Deutsche Forschungsgemeinschaft under grant GO 563/21-1. YH has been partially supported by the ISF (13/08). NIL acknowledges the support of the DFG and the hospitality of the KITP, supported in part by the National Science Foundation, under grant no. NSF PHY11-25915. AK is supported by the Spanish Ministerio de Ciencia e Innovación (MICINN) in Spain through the Ramon y Cajal programme as well as the grants AYA 2009-13875-C03-02, AYA2009-12792-C03-03, CSD2009-00064 and CAM S2009/ESP-1496. GY acknowledges support of MICINN (Spain) through research grants FPA2009-08958 and AYA2009-13875-C03-02 and through Consolider-Ingenio SyeC (CSD2007-0050). The simulations were performed at the Leibniz Rechenzentrum Munich (LRZ) and at Barcelona Supercomputing Center (BSC). We acknowledge the use of the CLUES data storage system EREBOS at AIP.

REFERENCES

Aragon-Calvo M. A., Szalay A. S., 2012, ArXiv e-prints
Aragón-Calvo M. A., Jones B. J. T., van de Weygaert R., van der Hulst J. M., 2007, A&A, 474, 315
Arnold V. I., Shandarin S. F., Zeldovich I. B., 1982, Geophys. Astrophys. Fluid Dyn., 20, 111
Avila Reese V., Colín P., Gottlöber S., Firmani C., Maulbetsch C., 2005, ApJ, 634, 51
Binney J., Tremaine S., 1987, Galactic Dynamics. Princeton Univ. Press, Princeton, NJ, p. 747
Blanton M. R., Eisenstein D., Hogg D. W., Schlegel D. J., Brinkmann J., 2005, ApJ, 629, 143
Bond J. R., Kofman L., Pogosyan D., 1996, Nat, 380, 603
Colberg J. M. et al., 2008, MNRAS, 387, 933
Dressler A., 1980, ApJ, 236, 351
Forero-Romero J. E., Hoffman Y., Gottlöber S., Klypin A., Yepes G., 2009, MNRAS, 396, 1815 (FR09)
Forero-Romero J. E., Hoffman Y., Yepes G., Gottoeber S., Piontek R., Klypin A., Steinmetz M., 2011, MNRAS, 417, 143
Gao L., Springel V., White S. D. M., 2005, MNRAS, 363, L66
Gunn J. E., Gott J. R., III, 1972, ApJ, 176, 1
Hahn O., Porciani C., Carollo C. M., Dekel A., 2007, MNRAS, 375, 489
Jasche J., Kitaura F. S., Li C., Enßlin T. A., 2010, MNRAS, 409, 355
Kitaura F. S., Jasche J., Li C., Enßlin T. A., Metcalf R. B., Wandelt B. D., Lemson G., White S. D. M., 2009, MNRAS, 400, 183
Kitaura F.-S., Angulo R. E., Hoffman Y., Gottlöber S., 2011, ArXiv e-prints
Klypin A. A., Shandarin S. F., 1983, MNRAS, 204, 891
Knebe A., Gill S. P. D., Gibson B. K., Lewis G. F., Ibata R. A., Dopita M. A., 2004, ApJ, 603, 7
Lee J., Lee B., 2008, ApJ, 688, 78
Lemson G., Kauffmann G., 1999, MNRAS, 302, 111
Libeskind N. I., Frenk C. S., Cole S., Helly J. C., Jenkins A., Navarro J. F., Power C., 2005, MNRAS, 363, 146
Libeskind N. I., Knebe A., Hoffman Y., Gottlöber S., Yepes G., Steinmetz M., 2011, MNRAS, 411, 1525
Libeskind N. I., Hoffman Y., Knebe A., Steinmetz M., Gottlöber S., Metuki O., Yepes G., 2012, MNRAS, 421, L137
Massey R. et al., 2007, Nat, 445, 286
Maulbetsch C., Avila-Reese V., Colín P., Gottlöber S., Khalatyan A., Steinmetz M., 2007, ApJ, 654, 53
Muñoz-Cuartas J. C., Mueller V., Forero-Romero J., 2011, MNRAS, 417, 1303
Novikov D., Colombi S., Doré O., 2006, MNRAS, 366, 1201
Sousbie T., Pichon C., Colombi S., Novikov D., Pogosyan D., 2008, MNRAS, 383, 1655
Wang H., Mo H. J., Yang X., van den Bosch F. C., 2012, MNRAS, 420, 1809
Zeldovich Y. B., 1970, A&A, 5, 84

This paper has been typeset from a TEX/LATEX file prepared by the author.